Rapid Communications

Prediction of a magnetic Weyl semimetal without spin-orbit coupling and strong anomalous Hall effect in the Heusler compensated ferrimagnet Ti_2MnAl

Wujun Shi,[1,2] Lukas Muechler,[3] Kaustuv Manna,[1] Yang Zhang,[1,4] Klaus Koepernik,[4,5] Roberto Car,[3] Jeroen van den Brink,[4] Claudia Felser,[1] and Yan Sun[1,*]

[1]*Max Planck Institute for Chemical Physics of Solids, D-01187 Dresden, Germany*
[2]*School of Physical Science and Technology, ShanghaiTech University, Shanghai 200031, China*
[3]*Department of Chemistry, Princeton University, Princeton, New Jersey 08544, USA*
[4]*Leibniz Institute for Solid State and Materials Research, 01069 Dresden, Germany*
[5]*IFW Dresden, P.O. Box 270116, D-01171 Dresden, Germany*

(Received 24 October 2017; revised manuscript received 11 February 2018; published 21 February 2018)

We predict a magnetic Weyl semimetal in the inverse Heusler Ti_2MnAl, a compensated ferrimagnet with a vanishing net magnetic moment and a Curie temperature of over 650 K. Despite the vanishing net magnetic moment, we calculate a large intrinsic anomalous Hall effect (AHE) of about 300 S/cm. It derives from the Berry curvature distribution of the Weyl points, which are only 14 meV away from the Fermi level and isolated from trivial bands. Different from antiferromagnets Mn_3X (X = Ge, Sn, Ga, Ir, Rh, and Pt), where the AHE originates from the noncollinear magnetic structure, the AHE in Ti_2MnAl stems directly from the Weyl points and is topologically protected. The large anomalous Hall conductivity (AHC) together with a low charge carrier concentration should give rise to a large anomalous Hall angle. In contrast to the Co-based *ferromagnetic* Heusler compounds, the Weyl nodes in Ti_2MnAl do not derive from nodal lines due to the lack of mirror symmetries in the inverse Heusler structure. Since the magnetic structure breaks spin-rotation symmetry, the Weyl nodes are stable without SOC. Moreover, because of the large separation between Weyl points of opposite topological charge, the Fermi arcs extent up to 75% of the reciprocal lattice vectors in length. This makes Ti_2MnAl an excellent candidate for the comprehensive study of magnetic Weyl semimetals. It is the first example of a material with Weyl points, large anomalous Hall effect, and angle despite a vanishing net magnetic moment.

DOI: 10.1103/PhysRevB.97.060406

Introduction. Weyl semimetals (WSMs) are recently discovered topological states in condensed matter physics that have attracted extensive interest due to their novel physics and potential applications in spintronics [1–6]. In Weyl semimetals, conduction and valence bands linearly touch each other in three-dimensional momentum space at the Weyl points. The Weyl points behave as monopoles of the Berry curvature field with positive and negative (or left and right handed) chirality, which leads to nonclosed surface Fermi arcs connecting a pair of Weyl points with opposite chirality [7–21]. Besides topological surface Fermi arcs, WSMs also exhibit exotic transport phenomena, such as the chiral anomaly effect [22–25], the gravitational anomaly effect [26], strong intrinsic anomalous and spin Hall effects [27–29], large magnetoresistance [22–24,30–33], and even special catalytic activity [34].

The existence of Weyl points requires breaking of spin degeneracy, either by breaking inversion or time reversal symmetry (or both) [35]. Since the Berry curvature is odd under time reversal, Weyl points in the latter case can generate a strong anomalous Hall effect (AHE). Although the total magnetic moment vanishes, time-reversal symmetry is broken in compensated ferrimagnets. In contrast to antiferromagnets, bands in compensated ferrimagnets are spin split, which allows the existence of Weyl points even without spin-orbit coupling (SOC). Additionally, the Weyl points in compensated ferrimagnets lead to a strong AHE despite a zero net magnetic moment. Different from the noncollinear antiferromagnets Mn_3X (X = Ge, Sn, Ga, Ir, Rh, and Pt) [36–39], the AHE in compensated magnetic WSMs is topologically protected. If the Weyl nodes are close to the Fermi level and are isolated from trivial bands, the charge carrier density is expected to be very low, and a large anomalous Hall angle is naturally expected in these materials.

In this paper, we have theoretically studied an ideal time reversal symmetry breaking WSM in the inverse Heusler compound Ti_2MnAl with compensated magnetic structure, where the Weyl points are only 14 meV away from the Fermi energy. Owing to the large Berry curvature around the Weyl points, Ti_2MnAl has an intrinsic anomalous Hall conductivity (AHC) of around 300 S/cm and despite a zero net magnetic moment. In Ti_2MnAl the Weyl points do not derive from mirror symmetry protected nodal lines, due to the lack of mirror planes in the inverse Heusler structure. Rather, the Weyl points exist without taking into account SOC, in contrast to the recently predicted Weyl-points in ferromagnetic Co-based magnetic Heusler compounds, which possess nodal lines close to the Fermi level [40,41]. Since the nodal lines normally disperse in energy, the Co-based magnetic Heusler WSMs have higher bulk charge carrier density, which makes the detection of Weyl points related phenomena difficult. Due to the lower symmetry, Ti_2MnAl has a small charge carrier density of only

*ysun@cpfs.mpg.de

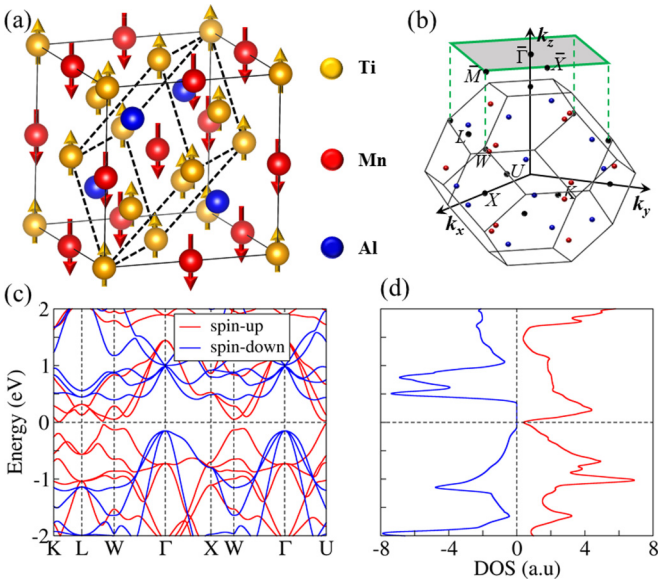

FIG. 1. (a) FCC lattice crystal structure of Ti_2MnAl. Spin polarizations of atom Mn and Ti are along positive and negative z direction, respectively. The primitive cell is marked by the dashed line. (b) Three-dimensional Brillouin zone (BZ) and its two-dimensional projection in the (001) direction. Weyl points with positive and negative chirality are presented by the red and blue spheres. (c),(d) Energy dispersion and density of states without inclusion of SOC. The labels of high symmetry points are given in (b).

2×10^{19} cm^3, which is even smaller than the charge carrier density in NbP [42]. Therefore the Weyl points in Ti_2MnAl should be much easier to observe experimentally and a large anomalous Hall angle AHA is expected. Heusler compounds are ideal materials for the study of the interplay between magnetism and topology [43,44] due to their excellent tunability. According to our calculations, Ti_2MnGa and Ti_2MnIn have a similar electronic structure with Weyl points. However, only Ti_2MnAl has been successfully grown in thin films with a high Curie temperature above 650 K [45,46]. Considering all these factors, Ti_2MnAl provides an excellent platform for the study of magnetic Weyl physics and suggests a new direction to obtain a strong AHE without a net magnetic moment.

Methods. To investigate the electronic band structure we have performed *ab initio* calculations based on density functional theory (DFT) using the full-potential local-orbital code (FPLO) [47] with a localized atomic basis and full potential treatment. The exchange and correlation energy was considered at the generalized gradient approximation (GGA) level [48] and GGA plus U with on site U of Ti-3d and Mn-3d orbital varying from 1 to 5 eV [49]. The tight binding model Hamiltonian was constructed by projecting the Bloch states onto atomic-orbital-like Wannier functions. By using the tight binding model Hamiltonian, we have calculated the surface state and intrinsic AHC.

Results. Ti_2MnAl has an inverse Heusler lattice structure with space group $F\bar{4}3M$ (No. 216) [Fig. 1(a)] [45,50], which, without the inclusion of spin-orbit coupling (SOC), shows a typical half metallic electronic band structure, as shown in Figs. 1(c) and 1(d). Because of the compensated magnetic

TABLE I. Location of one pair of Weyl points (labeled as W_A and W_B). Without inclusion of SOC, they are related to each other by the mirror plane, and all the other Weyl points can be obtained via the symmetries of $M_{\pm 110}$, $M_{1\pm 10}$, $M_{0\pm 11}$, $C_{2,x}$, $C_{2,y}$, and $C_{2,z}$. SOC breaks the mirror symmetry as a perturbation. A relevant high symmetry point near the Weyl point is the W point (0, 0.5, 1.0). The positions of Weyl points are described in the Cartesian coordinates in units of $(\frac{2\pi}{a}, \frac{2\pi}{a}, \frac{2\pi}{a})$.

	w/o SOC	SOC
W_A	(0, 0.4737, 0.7515)	(0, 0.4802, 0.7531)
W_B	(0.4737, 0, 0.7515)	(0.4680, 0, 0.7504)

sublattices formed by Ti and Mn, the net magnetic moment in Ti_2MnAl vanishes. The spin-down channel forms an insulating gap of 0.5 eV, and the spin-up channel is semimetallic, which is in good agreement with previous study [50]. The spin-up bands in Fig. 1(c) show an easily identifiable band anticrossing along the L-W direction, indicating a band inversion around the Fermi energy. Though there is a general gap for the spin-up channel along the high symmetry directions, its density of states is not zero at the Fermi level. Therefore, the spin-up bands should cut the Fermi level in some lower symmetry directions.

Indeed, there is a linear crossing point away from the high-symmetry lines (Table I). Due to the six mirror planes $M_{\pm 110}$, $M_{1\pm 10}$, and $M_{0\pm 11}$, together with the three rotation axes $C_{2,x}$, $C_{2,y}$, and $C_{2,z}$, there are 12 pairs of linear crossing points in total. This is completely different from the Co-based Heusler WSMs, where the band structures possess nodal lines without considering SOC. Calculating the Berry phases of these 12 pairs of linear crossing points, we found that half of them have Chern number $+1$ and the other half Chern number -1. Hence the chirality obeys the mirror symmetries, as presented in Fig. 1(b). The energy dispersion of one pair of Weyl points related by the mirror symmetry is given in Figs. 2(a) and 2(c), from which we can see that the Weyl points are just lying at the Fermi level.

In order to completely understand the Weyl points in Ti_2MnAl, we need to take SOC into consideration, though SOC is not very strong in this compound, due to the light elements involved. In the presence of SOC, the symmetry of the system is reduced and the details of band structures are dependent on the direction of the magnetization. To obtain the magnetic ground state, the total energies of magnetizations along the (001), (110), and (111) directions were compared. The net magnetic moments are still smaller than 1 $m\mu_B$ per formula unit and the total energy difference between them is smaller than 0.1 meV, which is beyond the accuracy of DFT itself. Taking the magnetic polarization along (001) as an example, we analyzed the band structures further. Since SOC is not so strong in this compound, it just acts as a weak perturbation. As it is well known, the existence of Weyl points only need the lattice translation symmetry, and they are robust as long as one pair of Weyl points with opposite chirality doesn't meet each other in the k space. The original position of one pair of Weyl points W_A and W_B and the energy dispersion slightly breaks the reflection symmetry $M_{\pm 110}$. A comparison of the

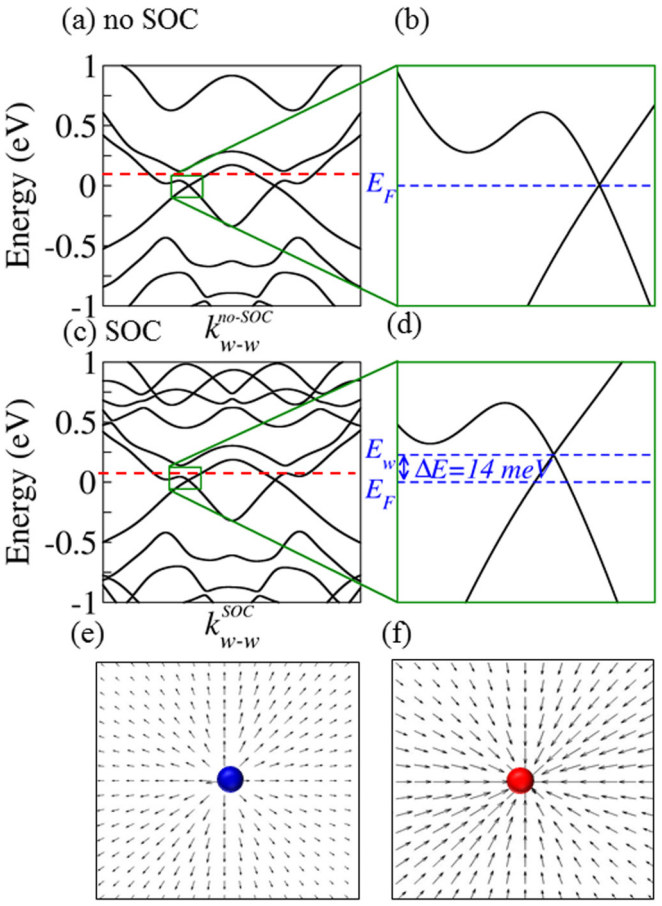

FIG. 2. (a)–(d) Energy dispersion of one pair of Weyl points for (a),(b) without and (c),(d) with inclusion of SOC. The red dashed lines in (a),(c) are the reference lines indicating the breaking of the mirror symmetries if SOC is considered. (e),(f) Berry curvature distribution around the Weyl points with positive and negative chirality.

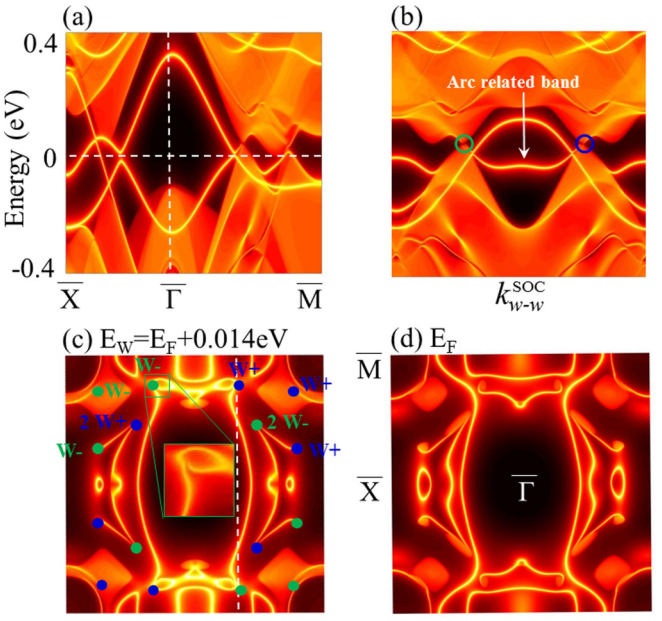

FIG. 3. Surface states of Ti_2MnAl terminated along the (001) direction. (a) Surface energy dispersion along high symmetry lines of $\overline{X}$-$\overline{\Gamma}$-$\overline{M}$. (b) Surface energy dispersion crossing one pair of Weyl points. The k path is given in (c). (c),(d) Fermi surface with energy lying at Weyl points and charge neutral point, respectively.

energy dispersions of one pair of Weyl points before and after the inclusion of SOC is shown in Figs. 2(a)–2(d). Without the inclusion of SOC, the energy dispersion is mirror symmetric, as shown by the red dashed line in Fig. 2(a). As long as SOC is taken into consideration, the mirror symmetry is not preserved. The bands corresponding to W_A cross the reference line (the red dashed line) two times, while the bands associated with W_B cross it four times. Because of the perturbation from SOC, the Weyl points are not at the charge neutrality point any more, which shifts them above the Fermi level by around 14 meV, see Fig. 2(d). Though the SOC slightly shifts the Weyl points in both momentum and energy, the chirality remains unchanged, as shown in Figs. 2(e) and 2(f). We found that the existence of Weyl points is robust after inclusion of on site U for Ti-3d and Mn-3d orbitals from 1 to 5 eV.

A typical feature of WSMs is the topological surface Fermi arc state. To calculate the (001) surface state, we considered an open boundary condition with the half-infinite surface by using iterative Green's function method [51,52]. From the energy dispersion along the high-symmetry line $\overline{X}$-$\overline{\Gamma}$-$\overline{M}$, surface bands connecting the bulk conduction and valence states can be seen, which should be related to the Fermi arcs. Actually, the two projected Weyl points on the (001) surface are very close to the $\overline{\Gamma}$-$\overline{M}$ line [see Figs. 3(c) and 3(d)], and therefore nearly linear bulk band crossings can be observed along $\overline{\Gamma}$-$\overline{M}$. Since Fermi arcs begin and end at the Weyl points with opposite chiralities, we have chosen a special direction along the two projected Weyl points [see Fig. 3(c)]. For the (001) surface, two Weyl points of the same chirality project onto each other. The corresponding energy dispersion, given in Fig. 3(b), clearly shows see the linear dispersion of the bulk Weyl points (labeled by the green and blue circles) with the Fermi arc related surface bands terminating at the two Weyl points. Because of the dispersion of the Fermi arcs below the Fermi level, they could be detected by ARPES and STM measurements.

By fixing the energy at the Weyl points, perfect Fermi arcs with tiny bulk states can clearly be seen in Fig. 3(c). Dependent on the number of surface projected Weyl points, the number of Fermi arcs terminated at each Weyl points differs. Moreover, two long Fermi arcs extend around 75% of the reciprocal lattice vector, which is amongst the longest Fermi arc to be observed so far. On shifting the energy down by 14 meV to the charge neutral point, there is slightly change in the surface state, and most of the Fermi arcs remain clearly detectable. Therefore, the Weyl semimetal states in Ti_2MnAl lead to the existence of isolated surface Fermi arcs, and the long Fermi arc around the charge neutral point should be easy to detect by surface techniques. Further, owing to the long Fermi arcs and small bulk charge carrier density, it is also easy to observe the Fermi arc induced quantum oscillation.

Owing to the large Berry curvature around the Weyl points, a strong AHE is expected in magnetic Weyl semimetals. To investigate the AHE we have computed the intrinsic AHC by the linear-response Kubo formula approach in the clean

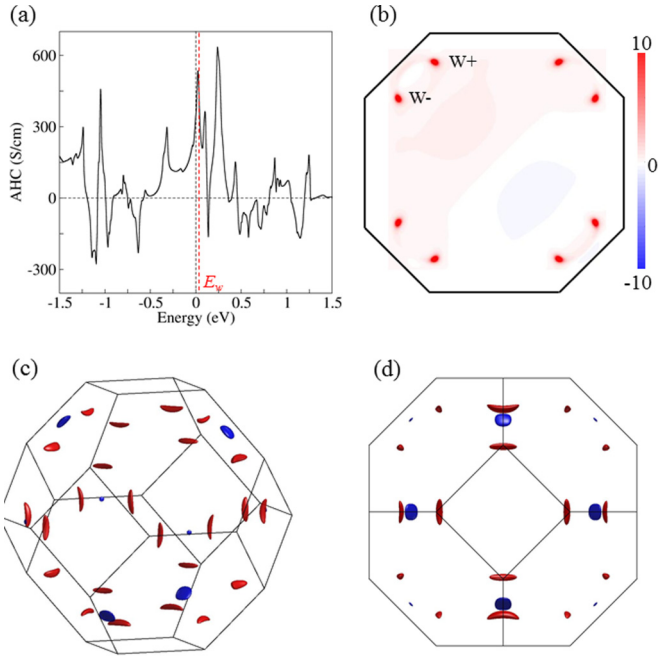

FIG. 4. (a) Energy dependent AHC. The peak value highlighted by red dashed line corresponds to the Weyl-node energy. (b) Berry curvature distribution in the $k_z = 0$ plane. The eight hot spots are just the positions of Weyl points. Color bars are arbitrary units. (c), (d) FSs distribution in the 3D BZ. Red and blue FSs are hole and electron bubbles, respectively.

limit [53]. A $500 \times 500 \times 500$ k grid in the BZ was used for the integral of the AHC.

If the magnetization is along the z axis, σ_{xy}^z is the only nonzero component of the AHC tensor. From our calculation, the intrinsic AHC is around 300 S/cm at the charge neutrality point. However, since the Weyl points are just above the Fermi level, the AHC should be sensitive to the position of chemical potential and a large value is expected at the energy of the Weyl points. To investigate the effect of electron and hole doping, we calculated the energy dependent AHC, see Fig. 4(a). The AHC increases sharply when shifting the energy from E_F to E_w, and the AHC attains a peak value at $E = E_w$ with $\sigma_{xy}^z = 550$ S/cm, implying that the large AHC originated from the Weyl points, since the Berry curvature distribution of a Weyl point peaks sharply at the nodal energy. For further confirmation of the effect of the Weyl points to the AHC, we analyzed the Berry curvature distribution in k space. Figure 4(b) shows the Berry curvature distribution in the $k_z = 0$ plane with four pairs of Weyl points very close to it. Except for the eight hot spots derived from the Weyl points, there are barely other contributions to the AHC. The other two high-symmetry planes $k_x = 0$ and $k_y = 0$ have almost the same Berry curvature distribution. Therefore, the AHE in Ti_2MnAl is mainly generated by the 12 pairs of Weyl points, and hence it is topologically protected.

The AHA, defined as $\sigma_{xy}^z/\sigma_{xx}$, provides a dimensionless measure of the strength of the AHE, which is the conversion efficiency from longitudinal charge current to transverse charge current. The longitudinal conductivity σ_{xx} is proportional to the charge carrier density and mobility. In comparison to metals, the charge carrier density of semimetals differs by some orders of magnitude and therefore the conductivity σ_{xx} is lower as well. Theoretically, the AHA can be estimated from the intrinsic AHC and charge carrier density. To evaluate the charge carrier density we have analyzed the FSs in three dimensions. As shown in Figs. 4(c) and 4(d), there are 24 electron bubbles and 8 hole bubbles in the first BZ, and all of them are very small. The charge carrier density obtained from the volume of the FSs is around 2×10^{19} cm^3, a typical semimetallic value. Though we cannot compute an accurate σ_{xx}, which needs further experimental transport measurements, a large AHA is expected from the small charge carrier density and a relatively large AHC. In the quantum anomalous Hall effect (QAHE), the AHA diverges, since the 2D bulk becomes insulating. A magnetic material with a large bulk AHA could show a QAHE in thin films due to quantum confinement [28], and therefore the study of thin film of Ti_2MnAl should be highly interesting.

Summary. In summary, we have theoretically predicted the magnetic WSM and large AHC in the inverse Heusler compound Ti_2MnAl with Weyl points only 14 meV away from the Fermi level. Because of the large Berry curvature from Weyl points and compensated magnetic structure, the strong AHE exists even without a net magnetic moment. Motivated by these findings, it would be interesting to investigate the topological properties of the other class of compensated ferrimagnets in the Heusler structure with 24 valence electrons [54]. Compared to noncollinear antiferromagnets Mn_3X (X = Ge, Sn, Ga, Ir, Rh, and Pt), Ti_2MnAl has much lower charge carrier density while the AHC is of similar magnitude, from which a large AHA and low energy consumption are also expected. Due to the large separation of Weyl points with opposite chirality, the Fermi arc extends up to 75% of the reciprocal lattice vectors in length. This work not only provides an excellent magnetic Weyl semimetal for both transport and surface study, but also suggests a direction for obtaining a large AHE without net magnetic moment.

Acknowledgments. This work was financially supported by the ERC Advanced Grant No. 291472 'Idea Heusler,' ERC Advanced Grant No. 742068–TOPMAT and Deutsche Forschungsgemeinschaft DFG under SFB 1143. R.C. and L.M. give thanks to DOE Grant No. DE-SC0017865. L.M. would like to thank the MPI CPFS for its hospitality where part of the work was performed.

W.S. and L.M. contributed equally to this paper.

[1] X. G. Wan, A. M. Turner, A. Vishwanath, and S. Y. Savrasov, Phys. Rev. B **83**, 205101 (2011).

[2] G. E. Volovik, *The Universe in A Helium Droplet* (Clarendon Press, Oxford, 2003).

[3] S. Murakami, New J. Phys. **10**, 029802 (2008).

[4] L. Balents, Physics **4**, 36 (2011).

[5] B. Yan and C. Felser, Annu. Rev. Condens. Matter Phys. **8**, 337 (2017).

[6] N. P. Armitage, E. J. Mele, and A. Vishwanath, Rev. Mod. Phys. **90**, 15001 (2018).

[7] S.-Y. Xu, I. Belopolski, N. Alidoust, M. Neupane, G. Bian, C. Zhang, R. Sankar, G. Chang, Y. Zhujun, C.-C. Lee, H. Shin-Ming, H. Zheng, J. Ma, D. S. Sanchez, B. Wang, A. Bansil, F. Chou, P. P. Shibayev, H. Lin, S. Jia, and M. Z. Hasan, Science **349**, 613 (2015).

[8] B. Q. Lv, H. M. Weng, B. B. Fu, X. P. Wang, H. Miao, J. Ma, P. Richard, X. C. Huang, L. X. Zhao, G. F. Chen, Z. Fang, X. Dai, T. Qian, and H. Ding, Phys. Rev. X **5**, 031013 (2015).

[9] L. X. Yang, Z. K. Liu, Y. Sun, H. Peng, H. F. Yang, T. Zhang, B. Zhou, Y. Zhang, Y. F. Guo, M. Rahn, D. Prabhakaran, Z. Hussain, S. K. Mo, C. Felser, B. Yan, and Y. L. Chen, Nat. Phys. **11**, 728 (2015).

[10] Z. K. Liu, L. X. Yang, Y. Sun, T. Zhang, H. Peng, H. F. Yang, C. Chen, Y. Zhang, Y. F. Guo, D. Prabhakaran, M. Schmidt, Z. Hussain, S.-K. Mo, C. Felser, B. Yan, and Y. L. Chen, Nat. Mater. **15**, 27 (2016).

[11] S.-Y. Xu, N. Alidoust, I. Belopolski, Z. Yuan, G. Bian, T.-R. Chang, H. Zheng, V. N. Strocov, D. S. Sanchez, G. Chang, C. Zhang, D. Mou, Y. Wu, L. Huang, C.-C. Lee, S.-M. Huang, B. Wang, A. Bansil, H.-T. Jeng, T. Neupert, A. Kaminski, H. Lin, S. J. Jia, and M. Z. Hasan, Nat. Phys. **11**, 748 (2015).

[12] I. Belopolski, S.-Y. Xu, D. S. Sanchez, G. Chang, C. Guo, M. Neupane, H. Zheng, C.-C. Lee, S.-M. Huang, G. Bian, N. Alidoust, T.-R. Chang, B. K. Wang, X. Zhang, A. Bansil, H.-T. Jeng, H. Lin, S. Jia, and M. Z. Hasan, Phys. Rev. Lett. **116**, 066802 (2016).

[13] N. Xu, H. M. Weng, B. Q. Lv, C. E. Matt, J. Park, F. Bisti, V. N. Strocov, D. Gawryluk, E. Pomjakushina, K. Conder, N. C. Plumb, M. Radovic, G. Autès, O. V. Yazyev, Z. Fang, X. Dai, T. Qian, J. Mesot, H. Ding, and M. Shi, Nat. Commun. **7**, 11006 (2016).

[14] S. Souma, Z. Wang, H. Kotaka, T. Sato, K. Nakayama, Y. Tanaka, H. Kimizuka, T. Takahashi, K. Yamauchi, T. Oguchi, K. Segawa, and Y. Ando, Phys. Rev. B **93**, 161112 (2016).

[15] H. Inoue, A. Gyenis, Z. Wang, J. Li, S. W. Oh, S. Jiang, N. Ni, B. A. Bernevig, and A. Yazdani, Science **351**, 1184 (2016).

[16] R. Batabyal, N. Morali, N. Avraham, Y. Sun, M. Schmidt, C. Felser, A. Stern, B. Yan, and H. Beidenkopf, Sci. Adv. **2**, e1600709 (2016).

[17] H. Zheng, S.-Y. Xu, G. Bian, C. Guo, G. Chang, D. S. Sanchez, I. Belopolski, C.-C. Lee, S.-M. Huang, X. Zhang, R. Sankar, N. Alidoust, T.-R. Chang, F. Wu, T. Neupert, F. Chou, H.-T. Jeng, N. Yao, A. Bansil, S. Jia, H. Lin, and M. Z. Hasan, ACS Nano **10**, 1378 (2016).

[18] A. A. Soluyanov, D. Gresch, Z. Wang, Q. Wu, M. Troyer, X. Dai, and B. A. Bernevig, Nature (London) **527**, 495 (2015).

[19] Y. Sun, S. C. Wu, M. N. Ali, C. Felser, and B. Yan, Phys. Rev. B **92**, 161107(R) (2015).

[20] H. Lei, K. Liu, J.-i. Yamaura, S. Maki, Y. Murakami, Z.-Y. Lu, and H. Hosono, Phys. Rev. B **93**, 121101(R) (2016).

[21] E. Haubold, K. Koepernik, D. Efremov, S. Khim, A. Fedorov, Y. Kushnirenko, J. van den Brink, S. Wurmehl, B. Buchner, T. K. Kim, M. Hoesch, K. Sumida, K. Taguchi, T. Yoshikawa, A. Kimura, T. Okuda, and S. V. Borisenko, Phys. Rev. B **95**, 241108(R) (2017).

[22] X. Huang, L. Zhao, Y. Long, P. Wang, D. Chen, Z. Yang, H. Liang, M. Xue, H. Weng, Z. Fang, X. Dai, and G. Chen, Phys. Rev. X **5**, 031023 (2015).

[23] C.-L. Zhang, S.-Y. Xu, I. Belopolski, Z. Yuan, Z. Lin, B. Tong, G. Bian, N. Alidoust, C.-C. Lee, S.-M. Huang, T.-R. Chang, G. Chang, C.-H. Hsu, H.-T. Jeng, M. Neupane, D. S. Sanchez, H. Zheng, J. Wang, H. Lin, C. Zhang, H.-Z. Lu, S.-Q. Shen, T. Neupert, M. Zahid Hasan, and S. Jia, Nat. Commun. **7**, 10735 (2016).

[24] Z. Wang, Y. Zheng, Z. Shen, Y. Zhou, X. Yang, Y. Li, C. Feng, and Z.-A. Xu, Phys. Rev. B **93**, 121112(R) (2016).

[25] A. C. Niemann, J. Gooth, S.-C. Wu, S. Bäßler, P. Sergelius, R. Hühne, B. Rellinghaus, C. Shekhar, V. Suß, M. Schmidt, C. Felser, B. Yan, and K. Nielsch, Sci. Rep. **7**, 43394 (2017).

[26] J. Gooth, A. C. Niemann, T. Meng, A. G. Grushin, K. Landsteiner, B. Gotsmann, F. Menges, M. Schmidt, C. Shekhar, V. Sueß, R. Huehne, B. Rellinghaus, C. Felser, B. Yan, and K. Nielsch, Nature **547**, 324 (2017).

[27] A. A. Burkov and L. Balents, Phys. Rev. Lett. **107**, 127205 (2011).

[28] G. Xu, H. Weng, Z. Wang, X. Dai, and Z. Fang, Phys. Rev. Lett. **107**, 186806 (2011).

[29] Y. Sun, Y. Zhang, C. Felser, and B. Yan, Phys. Rev. Lett. **117**, 146403 (2016).

[30] C. Shekhar, A. K. Nayak, Y. Sun, M. Schmidt, M. Nicklas, I. Leermakers, U. Zeitler, Y. Skourski, J. Wosnitza, Z. Liu, Y. Chen, W. Schnelle, H. Borrmann, Y. Grin, C. Felser, and B. Yan, Nat. Phys. **11**, 645 (2015).

[31] N. J. Ghimire, Y. Luo, M. Neupane, D. J. Williams, E. D. Bauer, and F. Ronning, J. Phys. Condens. Matter **27**, 152201 (2015).

[32] Y. Luo, N. J. Ghimire, M. Wartenbe, H. Choi, M. Neupane, R. D. McDonald, E. D. Bauer, J. Zhu, J. D. Thompson, and F. Ronning, Phys. Rev. B **92**, 205134 (2015).

[33] P. J. W. Moll, A. C. Potter, N. L. Nair, B. J. Ramshaw, K. A. Modic, S. Riggs, B. Zeng, N. J. Ghimire, E. D. Bauer, R. Kealhofer, F. Ronning, and J. G. Analytis, Nat. Commun. **7**, 12492 (2016).

[34] C. R. Rajamathi, U. Gupta, N. Kumar, H. Yang, Y. Sun, V. Suß, C. Shekhar, M. Schmidt, H. Blumtritt, P. Werner, B. Yan, S. Parkin, C. Felser, and C. N. R. Rao, Adv. Mater. **29**, 1606202 (2017).

[35] J. von Neumann and E. Wigner, Phys. Z. **30**, 465 (1929).

[36] H. Chen, Q. Niu, and A. H. MacDonald, Phys. Rev. Lett. **112**, 017205 (2014).

[37] A. K. Nayak, J. E. Fischer, Y. Sun, B. Yan, J. Karel, A. C. Komarek, C. Shekhar, N. Kumar, W. Schnelle, J. Ku bler, C. Felser, and S. S. P. Parkin, Sci. Adv. **2**, e1501870 (2016).

[38] S. Nakatsuji, N. Kiyohara, and T. Higo, Nature (London) **527**, 212 (2015).

[39] S. anisotropic anomalous Hall effect, G. I. R. spin Hall effect in the chiral antiferromagnetic compounds Mn 3 X (X = Ge, Sn, and Pt), Phys. Rev. B **95**, 075128 (2017).

[40] Z. W. Wang, M. G. Vergniory, S. Kushwaha, M. Hirschberger, and E. V. Chulkov, Phys. Rev. Lett. **117**, 236401 (2016).

[41] J. Kübler and C. Felser, EPL **114**, 47005 (2016).

[42] J. Klotz, S.-C. Wu, C. Shekhar, Y. Sun, M. Schmidt, M. Nicklas, M. Baenitz, M. Uhlarz, J. Wosnitza, C. Felser, and B. Yan, Phys. Rev. B **93**, 121105 (2016).

[43] S. Chadov, X. Qi, J. Kübler, G. H. Fecher, C. Felser, and S. C. Zhang, Nat. Mater. **9**, 541 (2010).

[44] C. Felser, G. H. Fecher, and B. Balked, Angew. Chem., Int. Ed. **46**, 668 (2007).

[45] W. Feng, X. Fu, C. Wan, Z. Yuan, X. Han, N. V. Quang, and S. Cho, Phys. Status Solidi RRL **9**, 641 (2015).

[46] Q.-L. Fang, J.-M. Zhang, and K.-W. Xu, J. Magn. Magn. Mater. **349**, 104 (2014).
[47] K. Koepernik and H. Eschrig, Phys. Rev. B **59**, 1743 (1999).
[48] J. P. Perdew, K. Burke, and M. Ernzerhof, Phys. Rev. Lett. **77**, 3865 (1996).
[49] S. L. Dudarev, G. A. Botton, S. Y. Savrasov, C. J. Humphreys, and A. P. Sutton, Phys. Rev. B **57**, 1505 (1998).
[50] S. Skaftouros, K. Ozdogan, E. Sasioglu, and I. Galanakis, Appl. Phys. Lett. **102**, 022402 (2013).
[51] M. P. L. Sancho, J. M. L. Sancho, and J. Rubio, J. Phys. F: Met. Phys. **14**, 1205 (1984).
[52] M. P. L. Sancho, J. M. L. Sancho, and J. Rubio, J. Phys. F: Met. Phys. **15**, 851 (1985).
[53] D. Xiao, M.-C. Chang, and Q. Niu, Rev. Mod. Phys. **82**, 1959 (2010).
[54] R. Stinshoff, A. K. Nayak, G. H. Fecher, B. Balke, S. Ouardi, Y. Skourski, T. Nakamura, and C. Felser, Phys. Rev. B **95**, 060410(R) (2017).